# Polaron Delocalization in Donor-Acceptor Polymers and its Impact on Organic Electrochemical Transistor Performance

Maximilian Moser,\* Achilleas Savva, Karl Thorley, Bryan D. Paulsen, Tania Cecilia Hidalgo, David Ohayon, Hu Chen, Alexander Giovannitti, Adam Marks, Nicola Gasparini, Andrew Wadsworth, Jonathan Rivnay, Sahika Inal and Iain McCulloch\*

M. Moser, Dr. A. Wadsworth, Prof. I. McCulloch University of Oxford, Department of Chemistry, Oxford, OX1 3TA UK

Corresponding authors: <a href="maximilian.moser@chem.ox.ac.uk">maximilian.moser@chem.ox.ac.uk</a> and <a href="maximilian.moser@chem.ox.ac.uk">iain.mcculloch@kaust.edu.sa</a>

Dr. A. Savva, T. C. Hidalgo, D. Ohayon, Prof. S. Inal King Abdullah University of Science and Technology (KAUST), Biological and Environmental Science and Engineering Division, Thuwal, 23955-6900, Saudi Arabia

Dr. K. Thorley University of Kentucky, Department of Chemistry, Lexington (KY), 40506-0055, USA

Dr. B. D. Paulsen, Prof. J. Rivnay Northwestern University, Department of Biomedical Engineering, Chicago (IL), 60208, USA

Dr. H. Chen, Prof. I. McCulloch King Abdullah University of Science and Technology (KAUST), Physical Science and Engineering Division, Thuwal, 23955-6900, Saudi Arabia

Dr. A. Giovannitti Stanford University, TomKatCenter for Sustainable Energy, Stanford (CA), 94305-4125, USA

Dr. A. Marks, Dr. N. Gasparini Imperial College London, Department of Chemistry and Center for Plastic Electronics, London, W12 0BZ, United Kingdom

Prof. J. Rivnay Northwestern University, Simpson Ouerrey Institute, Chicago (IL), 60611, USA

#### Keywords

Donor-acceptor copolymers, organic electrochemical transistors, polaron delocalization, polymers, semiconductors

#### Abstract

Donor-acceptor (D-A) polymers are promising materials for organic electrochemical transistors (OECTs), as they minimize detrimental faradaic side-reactions during OECT operation, yet their steady-state OECT performance still lags far behind their all-donor counterparts. Here, we report three D-A polymers based on the diketopyrrolopyrrole unit that afford OECT performances similar to those of all-donor polymers, hence representing a significant improvement to the previously developed D-A copolymers. In addition to improved OECT performance, DFT simulations of the polymers and their respective hole polarons also revealed a positive correlation between hole polaron delocalization and steady-state OECT performance, providing new insights into the design of OECT materials. More importantly, we demonstrate how polaron delocalization can be tuned directly at the molecular level by selection of the building blocks comprising the polymers' conjugated backbone, thus paving the way for the development of even higher performing OECT polymers.

#### Introduction

Polymer semiconductors which can support "mixed" ionic and electronic conduction have received considerable interest in the last decade due to their applicability in bioelectronic settings.<sup>[1–4]</sup> In this context, organic electrochemical transistors (OECTs), have been demonstrated to be a particularly successful device type, as highlighted by their use as neural recording elements, biomolecule sensors, cellular sensors and constituent components for neuromorphic applications.<sup>[5–13]</sup>

While advancements in device architecture have significantly contributed to the progress in OECTs,<sup>[14–16]</sup> the development of novel and carefully tailored channel materials has also been a crucial component for consistently reaching higher performances.<sup>[17–22]</sup> Amongst the several classes of OECT channel materials developed, ethylene glycol (EG) functionalized

organic semiconductors, have shown to be particularly promising candidates due to: (i) their lack of any insulating polyelectrolyte phase increasing the density of electronic charges that can be accumulated thus boosting their volumetric capacitance<sup>[21]</sup> (ii) their tendency to achieve optimum OECT performances without the need of any solvent-additives and post-processing treatments, [21,23] (iii) their excellent OECT operation, ranking them amongst the highest performing channel materials reported to date, [18,20,22,24], (iv) their good enzyme compatibility enabling for the direct detection of biologically relevant ions and molecules foregoing the need of any mediators and [10] and (v) their facile synthetic tunability at the molecular scale. Given the promise of EG functionalized organic semiconductors, several different molecular engineering strategies have been pursued to maximize their performance in OECTs. [25,26] Broadly speaking these can be categorized into those focusing on the modification of the side chains [22,27-32] and those altering the aromatic building blocks of the conjugated polymer backbone. [17-19,29,33,34] The efficacy of these modifications is typically assessed by comparing the maximum transconductance  $(g_m)$  that can be achieved in devices, see equation 1.

$$g_m = \mu C^* \cdot \frac{Wd}{L} (V_{TH} - V_G)$$
 Equation (1)

Where  $\mu$  is the electronic charge carrier mobility,  $C^*$  the volumetric capacitance, W the channel width, d the channel depth, L the channel length,  $V_{Th}$  the threshold voltage and  $V_G$  the gate voltage.

As illustrated in Equation 1, the maximum  $g_m$  that can be accomplished in devices is dependent on both device geometry (Wd/L) and material dependent  $([\mu C^*])$  terms. Consequently, a fairer comparison of the performance of different channel materials is accomplished by considering the  $[\mu C^*]$  of the various semiconductors. [24] Currently, the highest performing EG functionalized semiconductors for OECT applications are based on all-donor

backbones and can reach [ $\mu C^*$ ] up to ~500 F V<sup>-1</sup> cm<sup>-1</sup> s<sup>-1</sup>.[17,18,22] The performance of channel materials not featuring an all-donor but instead a donor-acceptor (D-A) polymer backbone, *e.g.* employing diketopyrrolopyrrole (DPP), isoindigo (IID), benzodithiophene (BDT), naphthalene tetracarboxylic diimide (NDI) or tetrafluorophenylene as the acceptor unit, [17,19,29,34–36] is however yet to match those of polythiophene based materials, with the reported [ $\mu C^*$ ] of materials typically ~10 F V<sup>-1</sup> cm<sup>-1</sup> s<sup>-1</sup>.[24,33] This class of materials has however been demonstrated to minimize noncapacitive faradaic side-reactions during OECT operation, thus preventing the formation of reactive and hazardous side-products that in turn are detrimental to OECT performance and safe operation.[34] As a result, there is a need to develop high-performance D-A copolymers for OECTs, in addition to the elucidation of broad structure-property relationships for the design of future high-performance D-A channel materials.

In this contribution we report the synthesis of three EG functionalized D-A copolymers for OECT applications, all of which are based on the DPP unit, see **Figure 1**. Following initial cyclic voltammetry (CV) measurements, we determined that each of the three polymers showed stable and reversible electrochemical switching in both aqueous and organic media, thus suggesting their suitability as channel materials for OECTs. Subsequent OECT fabrication and testing demonstrated that each of the polymers affords good OECT performances, incurring  $[\mu C^*]$  between 50-350 F cm<sup>-1</sup> V<sup>-1</sup> s<sup>-1</sup>, which compares well with the best performing all-donor based polymers. [17,18,24,28,31] Furthermore, we highlight how differences in the polymers' microstructure and degree of hole polaron delocalization directly impact the polymers' OECT mobility and hence performance. Specifically, we find that matching the relative electron density on the donor and acceptor moieties, *i.e.* reducing the energy level offset between the donor and acceptor units in D-A copolymers, is beneficial in terms of spreading the hole polaron over a larger proportion of the conjugated polymer backbone, which in turn boosts OECT mobility. On the other hand, we note that the operational stability of the polymers depends strongly on the overall electron density of the D-A polymer backbone, whereby the polymers

with higher electron densities, *i.e.* lower ionization potentials (*IP*) afford the highest operational stability. Consequently, we demonstrate how control over both the overall and relative energy levels in channel materials for OECTs is of utmost importance in terms of tuning their respective OECT steady-state performance and operational stability, thus providing valuable and generic guidelines for the design of stable high-performance D-A copolymers for OECT applications.

**Figure 1.** Chemical structures of p(gDPP-TT), p(gDPP-T2) and p(gDPP-MeOT2).

#### **Results and Discussion**

The thiophene flanked DPP core was synthesized according to literature procedures, condensation reaction between diethyl proceeding via succinate and thiophenecarbonitrile.<sup>[37]</sup> The DPP unit was subsequently functionalized with triethylene glycol chains and brominated to afford the central DPP monomer used in each of the subsequent polymerization reactions. Triethylene glycol chains were utilized as solubilizing groups in the synthesized polymers, as the vast majority of the glycolated semiconducting p-type channel materials reported to date employ these triethylene glycol units as side chains, thereby minimizing the impact of the side chain on the OECT performance and allowing for a better comparison between polymer backbones.<sup>[17,18,35,36,38]</sup> The dibrominated DPP monomer was then subjected to Stille cross-coupling polymerization to afford the polymers p(gDPP-TT), p(gDPP-T2) and p(gDPP-MeOT2) respectively, with their chemical structures illustrated in Figure 1. A

more detailed account of the synthetic procedures can be found in the supporting information (S.I.).

All polymers exhibited good solubility in chloroform, allowing for facile solution processing. Similar as for previously reported all EG functionalized DPP-based D-A copolymers, gel permeation chromatography (GPC) proved to be inconclusive affording unrealistically high molecular weights, potentially due to polymer aggregation in solution.<sup>[34]</sup> Although exact molecular weights could thus not determined for the polymers, the polymeric nature of the materials was evidenced by their similar <sup>1</sup>H NMR and UV-Vis spectra compared to their alkylated equivalents, *vide infra*.<sup>[39,40]</sup>

UV-vis absorption spectroscopy was performed on as cast polymer films, see **Figure S1** and **Figure S2** in the S.I. Each polymer exhibited a maximum absorption wavelength ( $\lambda_{max,film}$ ) above 800 nm, whereby p(gDPP-TT) and p(gDPP-T2) also featured relatively well-resolved vibronic features. The absorption profile of p(gDPP-MeOT2) on the other hand did not show any such features, indicating a higher degree of molecular ordering of p(gDPP-TT) and p(gDPP-T2) in the solid state. These results are in line with previous literature, in which the dimethoxybithiophene unit was also reported to lead to a loss in vibrational fine structure. The optical gap ( $E_{g,opt}$ ) for each polymer was calculated from the onset of absorption, incurring values of 1.22 eV, 1.22 eV and 0.96 eV for p(gDPP-TT), p(gDPP-T2) and p(gDPP-MeOT2) respectively. The bathochromically shifted  $\lambda_{max,film}$  and the smaller  $E_{g,opt}$  of p(gDPP-MeOT2) compared to p(gDPP-TT) and p(gDPP-T2) were attributed to the presence of the electron-donating methoxy substituents on the bithiophene unit in p(gDPP-MeOT2), which induced a reduced IP in the polymer.

**Table 1.** Optoelectronic properties of the polymers under investigation.

Dalyman	λ <sub>max,film</sub>	$E_{g,opt}$ $E_{ox,aq}$		$E_{ox,org}$	IP	
Polymer	[nm]	[eV]	$[V]^a$	$[\mathbf{V}]^b$	$[eV]^c$	
p(gDPP-TT)	833	1.22	+0.46	+0.12	5.11	
p(gDPP-T2)	812	1.22	+0.39	+0.04	5.03	
p(gDPP-MeOT2)	916	0.96	-0.14	-0.43	4.56	

a) Measured employing a 0.1 M NaCl<sub>(aq)</sub> solution as the supporting electrolyte; b) measured employing a 0.1 M solution of tetrabutylammonium hexafluorophosphate in acetonitrile as the supporting electrolyte; c) calculated from the  $E_{ox,org}$ .

Evaluation of the polymers' electrochemical properties was performed by CV in both organic and aqueous media. In both instances, a conventional three-electrode set up was employed, with the working electrode consisting of a polymer coated indium tin oxide (ITO) substrate, the counter electrode of a platinum wire and the reference electrode of an Ag/AgCl wire couple. The onset of oxidation in aqueous  $(E_{ox,aq})$  and organic  $(E_{ox,org})$  media, as well as the *IP* of the polymers are summarized in **Table 1**. The voltammograms corresponding to each polymer using an aqueous electrolyte can be found in Figure 2a, while those recorded employing an organic electrolyte in Figure S3 in the S.I. As shown in Figure 2a and Figure S3 the functionalization of each DPP derivative with the polar triethylene glycol side chains enabled reversible electrochemical switching in both organic and aqueous media, suggesting the suitability of these materials as channel materials for OECTs. As anticipated, p(gDPP-MeOT2) showed the lowest onset of oxidation, followed by p(gDPP-T2) and p(gDPP-TT). The IP calculated for p(gDPP-T2) and p(gDPP-TT) were also in good agreement with those calculated for their alkylated counterparts, [39,40] with minor variations in the recorded IP values attributed to differences in polymer-polymer and polymer-electrolyte interactions, which can lead to altered microstructures and ion penetration, which in turn affect IP values.<sup>[18]</sup> The trends in the onset of oxidation remained identical upon switching from an organic to an aqueous electrolyte, whereby a relatively large shift in oxidation potential was noted. Similar findings have been reported for alternative OECT channel materials; this was attributed to changes in

both the size and charge density of the counter anion and differences in the solute-solvent interactions between the polymer and the supporting electrolyte.<sup>[17,18,38,41–43]</sup>

Good agreement was found between the experimental *IP* and those calculated for tetramers of the polymers by range separated density functional theory calculations (IP-tuned ωB97XD/6-31G\*). Geometries were optimized in the gas phase and showed similar dihedral angles between common adjacent groups, see **Table S1** and **Figure S10** in the S.I. The thiophene-thiophene link in p(gDPP-MeOT2) is planarized by S-O non-covalent interactions, while the same dihedral in p(gDPP-T2) shows the typical 20° twist found between unsubstituted thiophenes. *IP* energies were calculated as the difference in electronic energy of radical cation and neutral states in an aqueous polarizable continuum, giving energies of 4.97, 5.00 and 4.67 eV for p(gDPP-TT), p(gDPP-T2) and p(gDPP-MeOT2) respectively. The similarity in *IP* between p(gDPP-TT) and p(gDPP-T2) can be explained by visualization of the molecular orbitals of the positive polaron species, see **Figure S11** in the S.I. The orbital, which was previously the highest occupied, but becomes unoccupied and with beta spin upon oxidation, shows delocalization over the DPP group and the adjoining thiophene rings. However, the equivalent orbital in p(gDPP-MeOT2) is localized on four thiophene rings instead due to the more electron rich nature, leading to a shift in the *IP*.

The kinetics of the doping/dedoping process occurring during CV, when employing an aqueous 0.1 M sodium chloride solution as the supporting electrolyte, were further evaluated by monitoring the anodic peak current ( $I_{max}$ ) against the scan rate (10-1250 mV s<sup>-1</sup>), whereby a negligible charge transfer resistance between the electrode and the polymer film was assumed. As shown in **Figure S4**, both p(gDPP-TT) and p(gDPP-T2) demonstrated a linear dependence on the scan rate up to 250 mV s<sup>-1</sup>. At scan rates higher than 250 mV s<sup>-1</sup> deviation from linearity for both polymers was noted with the dependence of the peak current on the scan rate appearing to assume a square root dependence on the scan rate, suggesting a diffusion limited current.<sup>[44,45]</sup> On the other hand, p(gDPP-MeOT2) showed a linear dependency of the peak current on the

scan rate across the entire probing regime (10-1250 mV s<sup>-1</sup>), suggesting that the dimethoxy moiety in the polymer is responsible for overcoming these kinetic limitations at high scan rates, giving this material a very rapid charge/discharge cycling properties. It is likely that the decreased molecular order in p(gDPP-MeOT2), as suggested by thin film UV-Vis data and grazing incidence wide-angle X-ray scattering measurements (discussed in more detail below), was responsible for this behavior, since in glycolated materials ionic mobility is higher in less ordered phases compared to more ordered or crystalline ones.<sup>[23,46]</sup> This property of p(gDPP-MeOT2) is likely to be particularly beneficial in the context of recording short-lived biological signals, such as neuronal action potentials.

The doping mechanism of the polymers was subsequently evaluated by means of spectroelectrochemistry. As shown in **Figure 2b-d**, p(gDPP-TT), p(gDPP-T2) and p(gDPP-MeOT2) all showed a significant electrochromic response upon the application of a positive bias to the polymer coated ITO electrode. For p(gDPP-TT) and p(gDPP-T2) both a suppression of the  $\pi$ - $\pi$ \* absorption band around 800 nm with the concomitant appearance of a new absorption feature at longer wavelengths was noted, eventually leading to the formation of an isosbestic point, whereby the longer wavelength absorbing features were related to the formation of polaronic/bipolaronic species of the polymer. As a decrease in the  $\pi$ - $\pi$ \* transition. Given, however, the similarity in the CV curves and the depression in the  $\pi$ - $\pi$ \* transition recorded across the three polymers, we speculate that p(gDPP-MeOT2) is also able to form analogous hole polarons upon applying a positive bias. The strong and reversible electrochromic response of these materials in aqueous media was viewed as a good indicator for the suitability of these materials as OECT channel materials, since both of these measurements rely upon the reversible electrochemical doping of the evaluated materials.

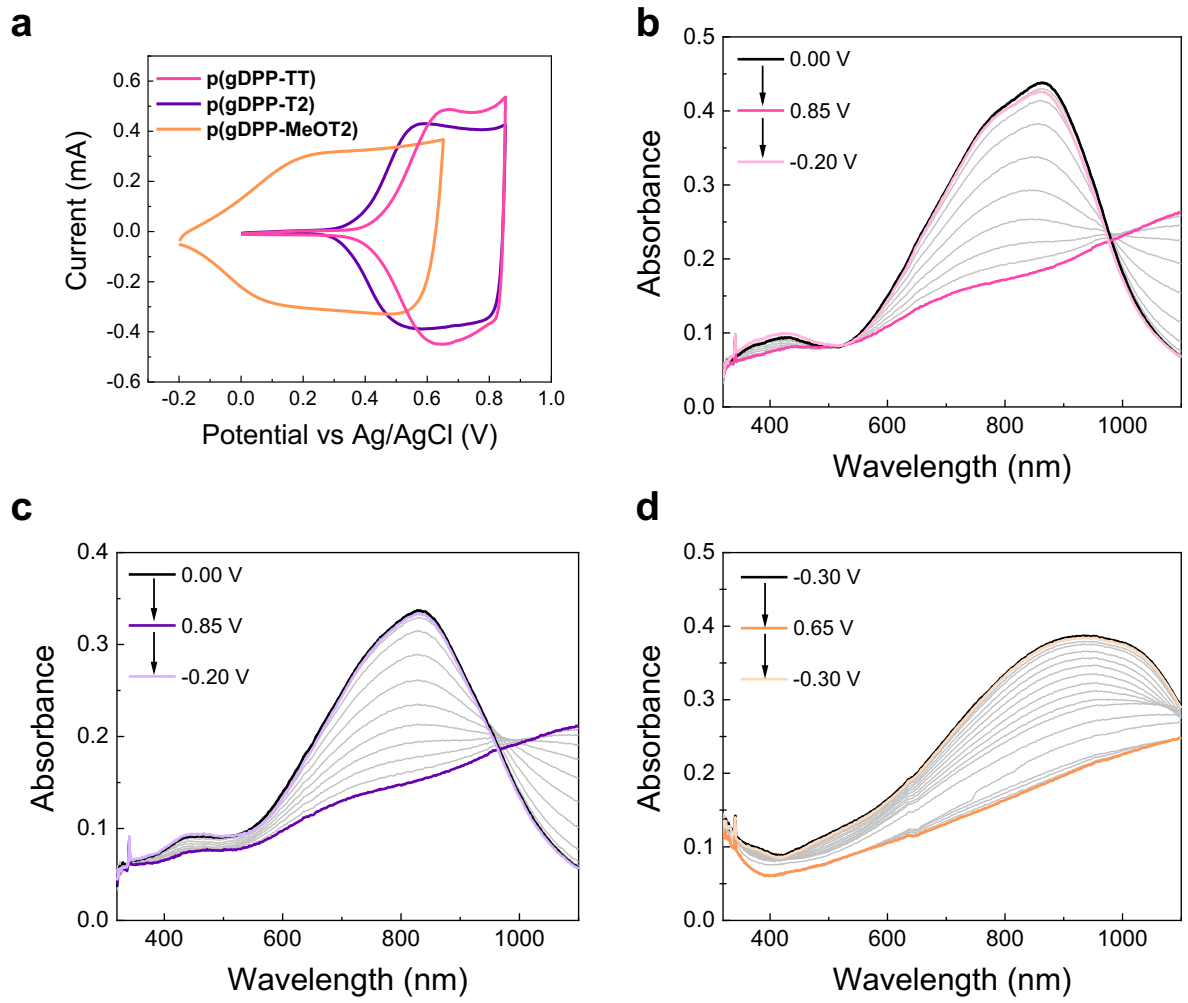


**Figure 2.** a) Cyclic voltammograms of p(gDPP-TT), p(gDPP-T2) and p(gDPP-MeOT2) employing a 0.1 M NaCl $_{(aq)}$  electrolyte. Spectroelectrochemical behavior of b) p(gDPP-TT), c) p(gDPP-T2) and d) p(gDPP-MeOT2) employing a 0.1 M NaCl $_{(aq)}$  electrolyte and working electrode potential steps of 0.05 V.

Following the complete electrochemical evaluation of these materials, their thermal properties were probed by thermogravimetric analysis (TGA) and differential scanning calorimetry (DSC). The TGA and DSC traces recorded for the three semiconductors are found in **Figure S5**. As can be seen, each material displayed excellent thermal stability up to 330 °C; while the lack of any features in the DSC traces indicated no significant morphological changes occurring when heating or cooling the samples. To further deepen our understanding of the structural properties of the materials, grazing incidence wide-angle X-ray scattering (GIWAXS) analysis was performed on spin-cast films of the polymers. As shown in **Figure S6**, all three polymers displayed a strong in-plane (010) peak from  $\pi$ - $\pi$  scattering and two clear orders of

out-of-plane lamellar scattering peaks, (100) and (200). This confirms the presence of a significant population of edge-on oriented crystallites. Peaks were fitted to extract peak positions and calculate d-spacings, shown in **Table 2**. The lamellar d-spacings, calculated from the (200) peak, were around 13 Å for all the polymers, implying either a high degree of torsion across each EG unit as predicted by the gauche effect or interdigitation of the triethylene glycol side chains. Similar  $\pi$ - $\pi$  stacking distances around 3.55±0.03 Å were obtained for p(gDPP-TT), p(gDPP-T2) and p(gDPP-MeOT2), which are comparable to the 3.5-3.6 Å sized  $\pi$ - $\pi$  stacking distances obtained for other high-performance EG functionalized organic semiconductors. <sup>[17,18]</sup> The pronounced lamellar and  $\pi$ - $\pi$  scattering peaks evidence a relatively high degree of order for an oligoethylene glycol side chain conjugated polymer. This was manifested in coherence lengths ( $L_c$ ) in the  $\pi$ - $\pi$  stacking direction, calculated from the FWHM of the (010) peak, of 10.2, 11.1, and 7.8 nm for p(gDPP-TT), p(gDPP-T2) and p(gDPP-MeOT2), respectively. <sup>[50]</sup>

Interestingly p(gDPP-TT) and p(gDPP-T2) both display a clear out of plane scattering peak at ~1.2 Å<sup>-1</sup>. It is not an integer multiple of the lamellar peak and being that it is in the out-of-plane direction it cannot be a backbone scattering peak from the main crystallite population. It may be from scattering related to the triethylene glycol side chains, similar to alkyl analogs, but as this is purely speculative the peak has not been indexed. [51,52] This peak is absent in the methoxy substituted p(gDPP-MeOT2). The presence of methoxy groups quantitatively disrupts the molecular packing, diminishing the  $\pi$ - $\pi$  stacking coherence length, consistent with the thin-film UV-vis spectra analysis that suggests a decreased molecular ordering relative to the other polymers in the series.

**Table 2.** GIWAXS analysis results of the polymers.

Polymer	Texture	Lamellar stacking		π-π stacking			
		$q_{(200)}$ (Å <sup>-1</sup> )	d (Å)	q <sub>(010)</sub> (Å <sup>-1</sup> )	d (Å)	$L_c$ (Å)	
p(gDPP-TT)	Edge-on	0.961	13.1	1.753	3.58	102.3	
p(gDPP-T2)	Edge-on	0.995	12.6	1.774	3.54	110.7	
p(gDPP-MeOT2)	Edge-on	0.933	13.5	1.784	3.52	78.4	

OECTs were fabricated according to previously reported methods, [53] resulting in channels with a 100  $\mu$ m width, 10  $\mu$ m length and similar thicknesses around 100 nm. In each case, the organic semiconductor was deposited by spin-coating without the need for any solvent additives or annealing treatments. Each device was operated employing a 0.1 M NaCl<sub>(aq)</sub> supporting electrolyte and an Ag/AgCl pellet gate electrode. Full details of the OECT fabrication and operating process can be found in the S.I. The output characteristics recorded for each polymer can be found in **Figure S7**, while the transfer and transconductance curves are reported in **Figure 3a-b**. The steady state *p*-type channel characteristics on the other hand are summarized in **Table 3**.

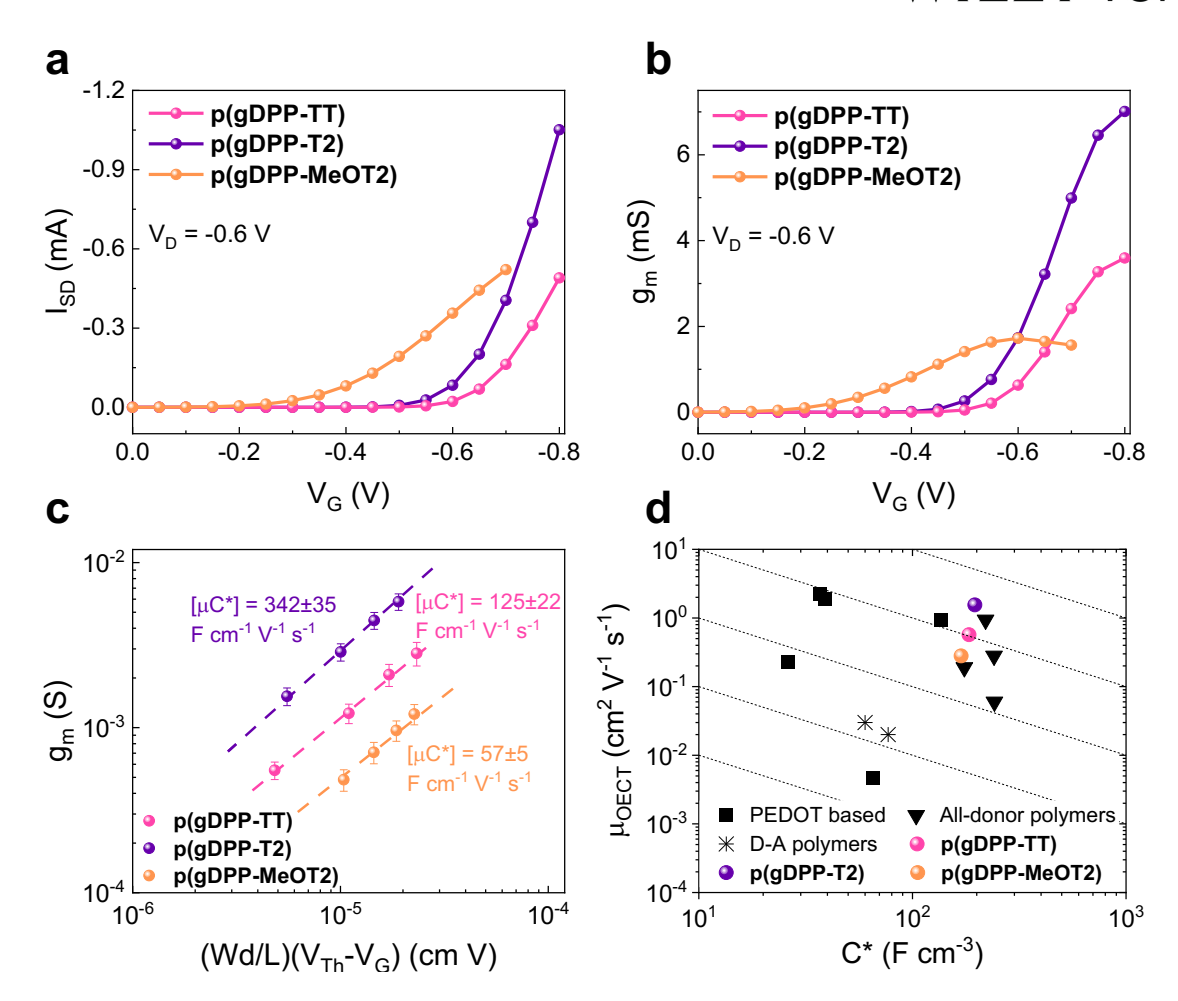


**Figure 3.** Representative a) transfer and b) transconductance curves recorded for a single channel of p(gDPP-TT), p(gDPP-T2) and p(gDPP-MeOT2) respectively. In each case a  $V_D$  sweep rate of 0.60 V s<sup>-1</sup> was employed. c) Extraction of  $[\mu C^*]$  from the transconductance against channel geometry and operation parameters plot. d) Comparison of the steady-state OECT performance of p(gDPP-TT), p(gDPP-T2) and p(gDPP-MeOT2) against other p-type OECT channel materials with reported  $\mu$  and  $C^*$  values. Data for PEDOT based materials taken from references [24] and [54], data for all-donor polymers taken from references [24], [28] and [31], data for D-A polymers taken from references [24] and [34].

**Table 3**. Summary of the steady-state characteristics recorded for OECTs fabricated with p(gDPP-TT), p(gDPP-T2) and p(gDPP-MeOT2).

Polymer	$\mathbf{g_m}^a$	$\mathbf{C}^{*b}$	$\mu_{\text{OECT}}^c$	$\mathbf{V}_{Th}$	$[\mu \mathbf{C}^*]^d$	d	On/
	(mS)	(F cm <sup>-3</sup> )	(cm <sup>2</sup> V <sup>-1</sup> s <sup>-1</sup> )	<b>(V)</b>	(F cm <sup>-1</sup> V <sup>-1</sup> s <sup>-1</sup> )	(nm)	off
p(gDPP-TT)	3.1±0.5	184	$0.57\pm0.09$	-0.54	125±22	123	10 <sup>5</sup>
p(gDPP-T2)	$6.3 \pm 0.7$	196	1.55±0.17	-0.52	342±35	90	$10^{5}$
p(gDPP-MeOT2)	1.4±0.2	169	$0.28 \pm 0.04$	-0.26	57±5	82	$10^{4}$

a) Averaged values over all operational channels on the same device; b) values calculated from EIS curves; c) calculated from the transistor saturation mobility using the respective  $C^*$  values; d) calculated from the slope of  $g_m$  as a function of  $[(Wd/L)(V_{Th}-V_G)]$ .

As shown in Figure 3a-b, each of the polymers studied operates in accumulation mode with the devices being off at a  $V_G$  of 0 V and switching on upon the application of a negative gate voltage. The average maximum transconductance recorded for p(gDPP-T2), p(gDPP-TT) and p(gDPP-MeOT2) was 6.3±0.7 mS, 3.1±0.5 mS and 1.4±0.2 mS respectively and occurred at a  $V_G$  of -0.8 V, -0.8 V and -0.6 V respectively. The drain current recorded for p(gDPP-T2) and p(gDPP-TT) became unstable at gate voltages lower than -0.8 V, thus meaning that the reported maximum transconductance values are those affording the maximum stable transconductance. The higher  $V_G$  required for p(gDPP-T2) and p(gDPP-TT) to reach their maximum transconductance were expected due to their higher IP, thus resulting in the devices to turn 'on' at more negative  $V_G$ . This trend was further reflected in the recorded  $V_{Th}$ , which followed the order of the polymers'  $E_{ox,aq}$ . A consequence of the polymers' varying IP and  $V_{Th}$ were the on-off ratios and off currents recorded for OECTs based on the various polymers, which have previously been employed to evaluate the propensity of polymers to undergo any spontaneous oxygen reduction reaction (ORR).<sup>[34]</sup> Devices based on each polymer afforded onoff ratios in the order of 10<sup>4</sup>-10<sup>5</sup>, see **Figure S8**, and were thus within the same range as those reported for previously developed all-donor and D-A polymers. [17,18,31,33,34] The slightly better on-off ratios obtained for p(gDPP-T2) and p(gDPP-TT) stemmed from their larger IP, >4.9 eV, thereby thermodynamically disfavoring any spontaneous ORR.

To exclude any channel geometry effects, thus enabling for a fair and material dependent comparison of the steady-state performance of each polymer, the polymers' [ $\mu C^*$ ] were measured, see Figure 3c.<sup>[24]</sup> The [ $\mu C^*$ ] recorded were 342±35 F cm<sup>-1</sup> V<sup>-1</sup> s<sup>-1</sup>, 125±22 F cm<sup>-1</sup> V<sup>-1</sup> s<sup>-1</sup> and 57±5 cm<sup>-1</sup> V<sup>-1</sup> s<sup>-1</sup> for p(gDPP-T2), p(gDPP-TT) and p(gDPP-MeOT2) respectively. As can be seen, p(gDPP-T2) incurred the highest steady-state OECT performance of the series, followed by p(gDPP-TT) with a slightly lower one. p(gDPP-MeOT2) on the other hand incurred the lowest steady-state OECT performance, roughly six-times lower than that of p(gDPP-T2). A comparison of the polymers' steady-state performance with those of previously published p-

D-A copolymers, is shown in **Figure 3d**. Figure 3d reveals that all of the three D-A polymers developed in this study perform significantly better than the previously reported D-A copolymers, affording similar steady-state performances to the all-donor polymers. Figure 3d also indicates that p(gDPP-T2) is one of the currently highest performing OECT channel materials.<sup>[21,22,24]</sup> Note that the steady-state performance of p(gDPP-T2) was obtained without any additives or post-processing treatment, which is often required for other high-performing channel materials.<sup>[21,23]</sup>

To better understand the origin of the performance difference across the channel materials reported in this study, we decided to individually compare their  $C^*$  and  $\mu$ .  $C^*$  was obtained from electrochemical impedance spectroscopy (EIS) of polymer coated gold electrodes while applying a gate voltage corresponding to the  $V_G$  incurring the highest  $g_m$ , see **Figure S9** in the S.I. For each of the polymers, a similar  $C^*$  of ~180 F cm<sup>-3</sup> was recorded, indicating that each polymer can reach similar levels of bulk doping in aqueous electrolytes. In comparison to the previously reported p-type active layer materials, the values obtained for  $C^*$  herein are amongst the highest. It is also worthwhile to note that these  $C^*$  values are around 50-400% higher than those of the commonly employed PEDOT derivatives. [24]

Given the similar  $C^*$  achieved by the various polymers, the difference in their steady-state performance was assumed to be a consequence of their differing charge carrier mobilities. This hypothesis was confirmed by the mobility values reported in Table 3, with p(gDPP-T2) showing the highest  $\mu$  of  $1.55\pm0.17$  cm<sup>2</sup> V<sup>-1</sup> s<sup>-1</sup>, while p(gDPP-TT) and p(gDPP-MeOT2) revealed lower values of  $0.57\pm0.09$  cm<sup>2</sup> V<sup>-1</sup> s<sup>-1</sup> and  $0.28\pm0.04$  cm<sup>2</sup> V<sup>-1</sup> s<sup>-1</sup> respectively. Given the previous findings from thin-film UV-vis absorption spectroscopy and GIWAXS analysis on the polymers, the higher charge carrier mobilities recorded for p(gDPP-T2) and p(gDPP-TT) were attributed in part to their higher degree of molecular order. Further insights into the higher  $\mu$  recorded for p(gDPP-T2) and p(gDPP-TT) came from DFT calculations (tuned

ωB97XD/6-31G\*), beginning with a population analysis of the polymers' molecular orbitals. This approach has previously been used in the literature to explain differences in the redox stability of glycolated semiconductors for OECT applications. [33,34] Key aspects of these computational simulations are the necessity to first optimize the polymer geometry in the gas phase, before optimizing the range separation parameter, ω, to satisfy Koopmans' theorem. This provides a realistic description of the charge delocalization and avoids the overdelocalization errors of standard DFT functionals. The tetrameric polymer chains were then subdivided into shorter fragments to determine the contribution of each fragment to the orbital under consideration. The tetrameric polymer species were optimized in the gas phase at the ωB97XD/6-31G\* level. Polymer fragments were subsequently defined analogously to a previous study on OECT channel materials, see **Figure 4a**, thus facilitating a comparison of the DFT simulations across both sets of polymers. [34]

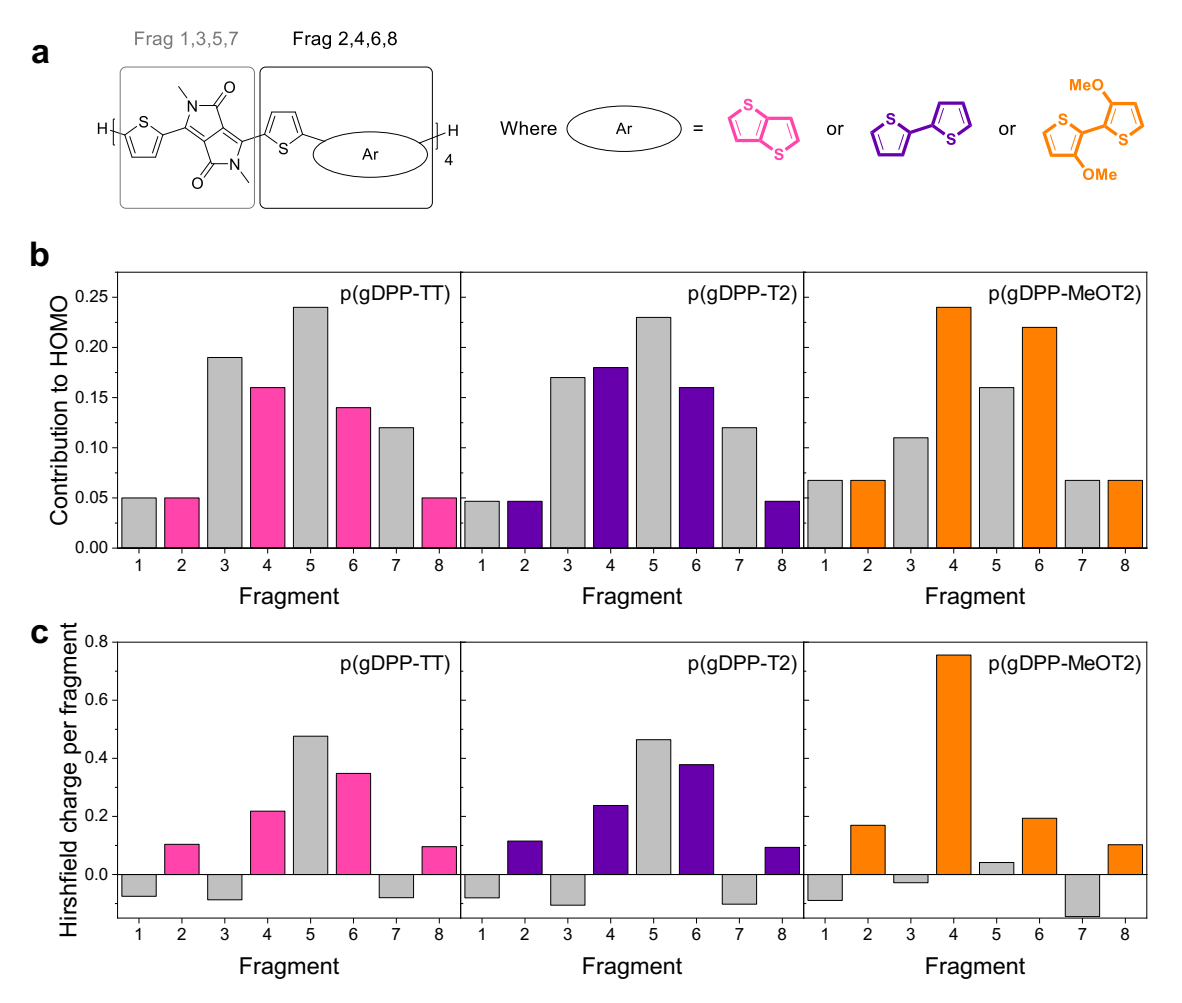


**Figure 4**. a) Details regarding the fragmentation of the polymer chains into shorter segments; DFT calculations of the b) HOMO orbital contribution of the various polymer fragments and c) charge distribution over the various polymer fragments in the polymers' radical cation form.

As can be seen from **Figure 4b**, p(gDPP-TT) and p(gDPP-T2) show similar orbital distributions of their neutral polymer HOMO, with the HOMO having strong contributions over five fragments (3-7). Conversely, p(gDPP-MeOT2) demonstrates a narrower HOMO distribution, only extending over four fragments (3-6), suggesting a higher degree of localization of the wavefunction. Moreover, whereas both p(gDPP-TT) and p(gDPP-T2) display stronger contributions of the DPP-based fragments towards the HOMO, this is not the case for p(gDPP-MeOT2), where the aryl (Ar) comonomer fragment dominates the orbital contribution. Summation of the fragment orbital distributions further highlights this concept, whereby the incorporation of the MeOT2 unit in p(gDPP-MeOT2) (60% Ar, 40% DPP) inverted the orbital contribution relative to p(gDPP-TT) (40% Ar, 60% DPP) and p(gDPP-T2) (43% Ar,

57% DPP). Similar findings were obtained for the vacant beta spin orbital of the radical cation, see Figure S12 in the S.I. and were reaffirmed by Hirshfield charge analyses of the radical cation form of the polymer, which has previously been used to model the polymers' polaronic species.<sup>[34]</sup> As follows from **Figure 4c** the charge in p(gDPP-TT) and p(gDPP-T2) was spread to a greater extent and more evenly as compared to p(gDPP-MeOT2), where the positive charge of the polymer resides almost entirely on a single fragment (4). More delocalized polarons may contribute to higher charge mobility in two ways; firstly both intra- and inter-chain mobility is expected to increase as the charge is spread out over more atoms, resulting in lower polaron binding energy.<sup>[55]</sup> Secondly, the increased spread of charge provides a larger surface area for charges to hop to adjacent polymer chains, increasing the interchain charge mobility. The above analysis thus suggests a more delocalized nature of the polaron in p(gDPP-T2) and p(gDPP-TT) compared to p(gDPP-MeOT2), which was attributed to the closer energy match between the T2 and TT moieties with the DPP unit compared to MeOT2. This aspect is particularly interesting to note for the molecular design of future conjugated polymers for OECT applications featuring a D-A conjugated backbone, as it would suggest that donor and acceptor units that are more closely matched in terms of their electron-densities and hence energy levels, should partially be responsible for yielding materials with better charge transport properties. This hypothesis could potentially also form part of the explanation why a higher  $\mu$  of 0.28±0.04 cm<sup>2</sup> V<sup>-1</sup> s<sup>-1</sup> was recorded for p(gDPP-MeOT2) compared to its pyridine-flanked DPP analogue, p(gPvDPP-MeOT2), for which a  $\mu$  of 0.030±0.007 cm<sup>2</sup> V<sup>-1</sup> s<sup>-1</sup> was reported.<sup>[34]</sup> A fair comparison can be made between these materials, especially given that the two polymers featured very similar degrees of lamellar ordering and  $\pi$ - $\pi$  stacking distances (both around 3.5) Å), as well as a lack of any significant vibronic fine-structure in their UV-vis thin film spectra. We speculate that this design concept of reducing the energy level offset between the donor and acceptor fragments may also hold true for *n*-type OECT polymers, thus explaining the higher OECT mobility achieved by the all-acceptor polymer BBL over the naphthalene bisimide-co-

bithiophene (NDI-T2) based D-A copolymers reported up-to-date.<sup>[19,27,56]</sup> Finally, this could also partially explain why all-donor based glycolated polymers have thus far been very successful *p*-type OECT channel materials, given the closer match in energy levels between their comonomers.<sup>[17,18,22]</sup>

Having fully characterized the steady-state performance of the OECTs fabricated with the various polymers, device operational stability was evaluated next. In this context, the percentage retention of the initial current as a function of OECT switching cycles  $(I_D/I_{D,\theta})$  is typically employed as figure-of-merit.[18,22,34,35,56,57] Consequently, we chose to also evaluate the operational stability of our materials by this metric. Specifically, this involved switching the devices between their 'on' and 'off' state for 5 s each and measuring the  $I_D/I_{D,\theta}$  over 100 min of continuous electrochemical cycling (~600 doping/dedoping cycles). To best compare the operational stability of the polymers, we wanted to ensure that similar doping levels were achieved within each polymer in their 'on' state. [58] Consequently, the  $V_G$  applied for the various polymers was -0.1 V smaller than their corresponding  $V_{Th}$ . The operational stability of the polymers is summarized in Figure S13. Figure S13 demonstrates that the polymers had significantly different electrochemical cycling profiles, with p(gDPP-TT), p(gDPP-T2) and p(gDPP-MeOT2) incurring 9%, 53% and 99% retention of the initial 'on' current after 100 min of continuous electrochemical cycling. The relative operational stability of the polymers under long-term cycling was ascribed to the different overall electron density on the polymer backbones', i.e. the polymers' IPs, whereby decreasing the polymers' IP resulted in progressively more stable devices due to better stabilization of the resulting hole polaron, thus corroborating previous literature findings.[33,34,58]

#### Conclusion

In summary, three polymers for accumulation mode p-type OECTs have been developed, all of which were based on a common diketopyrrolopyrrole unit. As confirmed by

CV, each of the synthesized polymers can undergo stable and reversible doping, hence suggesting the suitability of the diketopyrrolopyrrole moiety for OECTs. This was further confirmed by spectroelectrochemistry, which indicated a reversible suppression in the  $\pi$ - $\pi$ \* transition and a concomitant formation of an absorption feature at longer wavelengths, which was indicative of the reversible formation of charged species of the polymers.

GIWAXS analysis of the materials highlighted their semicrystalline nature, whereby p(gDPP-T2) and p(gDPP-TT) were found to display a higher degree of order compared to p(gDPP-MeOT2). These findings were further reflected in thin-film UV-Vis spectroscopy, with p(gDPP-T2) and p(gDPP-TT) both showing vibrational fine-structures in their absorption spectra, that were absent in the case of p(gDPP-MeOT2).

Subsequent OECT fabrication and analysis demonstrated good OECT performance for each of the materials developed, incurring [ $\mu$ C\*] values between 57-342 F cm<sup>-1</sup> V<sup>-1</sup> s<sup>-1</sup>, which compare well with the highest performing ethylene glycol functionalized semiconductors reported to date and represent a significant improvement to previously developed D-A copolymers for OECTs. Out of the polymers developed, p(gDPP-T2) and p(gDPP-TT) performed the highest, whereby their increased performance was attributed partially to their higher degree of order in their solid state. Importantly, DFT simulations of the polymers indicated p(gDPP-T2) and p(gDPP-TT) to also have significantly more delocalized hole polarons compared to p(gDPP-MeOT2), which was ascribed to the closer energy level match between the T2 and TT units with the thiophene-flanked DPP core, compared to the MeOT2 comonomer. Consequently, these findings highlight the significance of the degree of delocalization of polarons in OECT channel materials. More importantly, we demonstrate how this aspect can be tuned directly at the molecular level by selection of the building blocks comprising the polymers' conjugated backbone, thus paving the way for the development of even higher performing D-A copolymers for OECT applications.

#### Acknowledgements

The authors acknowledge generous funding from KAUST for financial support. The research reported in this publication was sponsored by funding from King Abdullah University of Science and Technology Office of Sponsored Research (OSR) under awards no. OSR-2018-CARF/CCF-3079, no. OSR-2015-CRG4-2572 and OSR-4106 CPF2019. We acknowledge EC FP7 Project SC2 (610115), EC H2020 (643791), and EPSRC Projects EP/G037515/1, EP/M005143/1, and EP/L016702/1. B.P. and J.R. gratefully acknowledge support from the National Science Foundation Grant No. NSF DMR-1751308. The authors would like to thank Joseph Strzalka and Qingteng Zhang for beam line assistance. This research used resources of the Advanced Photon Source, a U.S. Department of Energy (DOE) Office of Science User Facility operated for the DOE Office of Science by Argonne National Laboratory under Contract No. DE-AC02-06CH11357.

#### References

- [1] R. M. Owens, G. G. Malliaras, MRS Bull. 2010, 35, 449.
- [2] J. Rivnay, R. M. Owens, G. G. Malliaras, *Chem. Mater.* **2014**, *26*, 679.
- [3] D. T. Simon, E. O. Gabrielsson, K. Tybrandt, M. Berggren, Chem. Rev. 2016, 116, 13009.
- [4] B. D. Paulsen, K. Tybrandt, E. Stavrinidou, J. Rivnay, *Nat. Mater.* **2020**, *19*, 13.
- [5] X. Strakosas, M. Bongo, R. M. Owens, J. Appl. Polym. Sci. 2015, 132, 41735.
- [6] D. Khodagholy, T. Doublet, P. Quilichini, M. Gurfinkel, P. Leleux, A. Ghestem, E. Ismailova, T. Hervé, S. Sanaur, C. Bernard, G. G. Malliaras, *Nat. Commun.* 2013, 4, 1575.
- [7] A. Campana, T. Cramer, D. T. Simon, M. Berggren, F. Biscarini, *Adv. Mater.* **2014**, *26*, 3874.
- [8] C. Liao, C. Mak, M. Zhang, H. L. W. Chan, F. Yan, Adv. Mater. 2015, 27, 676.

- [9] A. M. Pappa, V. F. Curto, M. Braendlein, X. Strakosas, M. J. Donahue, M. Fiocchi, G.
  G. Malliaras, R. M. Owens, *Adv. Healthc. Mater.* 2016, 5, 2295.
- [10] A. M. Pappa, D. Ohayon, A. Giovannitti, I. P. Maria, A. Savva, I. Uguz, J. Rivnay, I. McCulloch, R. M. Owens, S. Inal, Sci. Adv. 2018, 4, 0911.
- [11] J. Rivnay, M. Ramuz, P. Leleux, A. Hama, M. Huerta, R. M. Owens, *Appl. Phys. Lett.*2015, 106, 043301.
- [12] P. Gkoupidenis, N. Schaefer, B. Garlan, G. G. Malliaras, Adv. Mater. 2015, 27, 7176.
- [13] J. Y. Gerasimov, R. Gabrielsson, R. Forchheimer, E. Stavrinidou, D. T. Simon, M. Berggren, S. Fabiano, Adv. Sci. 2019, 6, 1801339.
- [14] G. D. Spyropoulos, J. N. Gelinas, D. Khodagholy, Sci. Adv. 2019, 5, aau7378.
- [15] M. J. Donahue, A. Williamson, X. Strakosas, J. T. Friedlein, R. R. McLeod, H. Gleskova,G. G. Malliaras, *Adv. Mater.* 2018, *30*, 1705031.
- [16] A. F. Paterson, H. Faber, A. Savva, G. Nikiforidis, M. Gedda, T. C. Hidalgo, X. Chen, I. McCulloch, T. D. Anthopoulos, S. Inal, Adv. Mater. 2019, 31, 1902291.
- [17] C. B. Nielsen, A. Giovannitti, D. T. Sbircea, E. Bandiello, M. R. Niazi, D. A. Hanifi, M. Sessolo, A. Amassian, G. G. Malliaras, J. Rivnay, I. McCulloch, *J. Am. Chem. Soc.* 2016, 138, 10252.
- [18] A. Giovannitti, D. T. Sbircea, S. Inal, C. B. Nielsen, E. Bandiello, D. A. Hanifi, M. Sessolo, G. G. Malliaras, I. McCulloch, J. Rivnay, *Proc. Natl. Acad. Sci. U. S. A.* 2016, 113, 12017.
- [19] A. Giovannitti, C. B. Nielsen, D. T. Sbircea, S. Inal, M. Donahue, M. R. Niazi, D. A. Hanifi, A. Amassian, G. G. Malliaras, J. Rivnay, I. McCulloch, *Nat. Commun.* **2016**, *7*, 13066.
- [20] C. G. Bischak, L. Q. Flagg, K. Yan, C. Z. Li, D. S. Ginger, ACS Appl. Mater. Interfaces 2019, 11, 28138.
- [21] S. M. Kim, C. H. Kim, Y. Kim, N. Kim, W. J. Lee, E. H. Lee, D. Kim, S. Park, K. Lee,

- J. Rivnay, M. H. Yoon, *Nat. Commun.* **2018**, *9*, 3858.
- [22] M. Moser, T. C. Hidalgo, J. Surgailis, J. Gladisch, S. Ghosh, R. Sheelamanthula, Q. Thiburce, A. Giovannitti, A. Salleo, N. Gasparini, A. Wadsworth, I. Zozoulenko, M. Berggren, E. Stavrinidou, S. Inal, I. McCulloch, *Adv. Mater.* 2020, 32, 2002748.
- [23] J. Rivnay, S. Inal, B. A. Collins, M. Sessolo, E. Stavrinidou, X. Strakosas, C. Tassone,
  D. M. Delongchamp, G. G. Malliaras, *Nat. Commun.* 2016, 7, 11287.
- [24] S. Inal, G. G. Malliaras, J. Rivnay, *Nat. Commun.* **2017**, *8*, 1767.
- [25] M. Moser, J. F. Ponder, A. Wadsworth, A. Giovannitti, I. McCulloch, *Adv. Funct. Mater.*2019, 29, 1807033.
- [26] E. Zeglio, O. Inganäs, Adv. Mater. 2018, 30, 1800941.
- [27] A. Giovannitti, I. P. Maria, D. Hanifi, M. J. Donahue, D. Bryant, K. J. Barth, B. E. Makdah, A. Savva, D. Moia, M. Zetek, P. R. F. Barnes, O. G. Reid, S. Inal, G. Rumbles, G. G. Malliaras, J. Nelson, J. Rivnay, I. McCulloch, *Chem. Mater.* 2018, 30, 2945.
- [28] L. Q. Flagg, C. G. Bischak, J. W. Onorato, R. B. Rashid, C. K. Luscombe, D. S. Ginger, J. Am. Chem. Soc. 2019, 141, 4345.
- [29] Y. Wang, E. Zeglio, H. Liao, J. Xu, F. Liu, Z. Li, I. P. Maria, D. Mawad, A. Herland, I. McCulloch, W. Yue, *Chem. Mater.* 2019, 31, 9797.
- [30] A. Savva, R. Hallani, C. Cendra, J. Surgailis, T. C. Hidalgo, S. Wustoni, R. Sheelamanthula, X. Chen, M. Kirkus, A. Giovannitti, A. Salleo, I. McCulloch, S. Inal, Adv. Funct. Mater. 2020, 30, 1907657.
- [31] P. Schmode, A. Savva, R. Kahl, D. Ohayon, F. Meichsner, O. Dolynchuk, T. Thurn-Albrecht, S. Inal, M. Thelakkat, *ACS Appl. Mater. Interfaces* **2020**, *12*, 13029.
- [32] M. Moser, L. R. Savagian, A. Savva, M. Matta, J. F. Ponder, T. C. Hidalgo, D. Ohayon, R. Hallani, M. Reisjalali, A. Troisi, A. Wadsworth, J. R. Reynolds, S. Inal, I. McCulloch, *Chem. Mater.* 2020, 32, 6618.
- [33] A. Giovannitti, K. J. Thorley, C. B. Nielsen, J. Li, M. J. Donahue, G. G. Malliaras, J.

- Rivnay, I. McCulloch, Adv. Funct. Mater. 2018, 28, 1706325.
- [34] A. Giovannitti, R. B. Rashid, Q. Thiburce, B. D. Paulsen, C. Cendra, K. Thorley, D. Moia, J. T. Mefford, D. Hanifi, D. Weiyuan, M. Moser, A. Salleo, J. Nelson, I. McCulloch, J. Rivnay, *Adv. Mater.* 2020, 32, 1908047.
- [35] A. Giovannitti, K. J. Thorley, C. B. Nielsen, J. Li, M. J. Donahue, G. G. Malliaras, J. Rivnay, I. McCulloch, *Adv. Funct. Mater.* **2018**, *28*, 1706325.
- [36] Z. S. Parr, R. Halaksa, P. A. Finn, R. B. Rashid, A. Kovalenko, M. Weiter, J. Rivnay, J. Krajčovič, C. B. Nielsen, *Chempluschem* 2019, 84, 1384.
- [37] M. Grzybowski, D. T. Gryko, Adv. Opt. Mater. 2015, 3, 280.
- [38] L. R. Savagian, A. M. Österholm, J. F. Ponder, K. J. Barth, J. Rivnay, J. R. Reynolds, *Adv. Mater.* **2018**, *30*, 1804647.
- [39] Y. Li, P. Sonar, S. P. Singh, M. S. Soh, M. Van Meurs, J. Tan, J. Am. Chem. Soc. 2011, 133, 2198.
- [40] Y. Li, S. P. Singh, P. Sonar, Adv. Mater. 2010, 22, 4862.
- [41] C. Cendra, A. Giovannitti, A. Savva, V. Venkatraman, I. McCulloch, A. Salleo, S. Inal,J. Rivnay, Adv. Funct. Mater. 2019, 29, 1807034.
- [42] A. M. Österholm, J. F. Ponder, M. De Keersmaecker, D. E. Shen, J. R. Reynolds, *Chem. Mater.* 2019, 31, 2971.
- [43] A. Savva, C. Cendra, A. Giugni, B. Torre, J. Surgailis, D. Ohayon, A. Giovannitti, I. McCulloch, E. Di Fabrizio, A. Salleo, J. Rivnay, S. Inal, *Chem. Mater.* **2019**, *31*, 927.
- [44] T. A. Skotheim, J. R. Reynolds, *Conjugated Polymers: Theory, Synthesis, Properties, and Characterization*, **2007**.
- [45] T. H. Le, Y. Kim, H. Yoon, *Polymers* **2017**, *9*, 150.
- [46] Z. Xue, D. He, X. Xie, J. Mater. Chem. A 2015, 3, 19218.
- [47] S. Garreau, G. Louarn, J. P. Buisson, G. Froyer, S. Lefrant, *Macromolecules* **1999**, *32*, 6807.

- [48] I. Zozoulenko, A. Singh, S. K. Singh, V. Gueskine, X. Crispin, M. Berggren, *ACS Appl. Polym. Mater.* **2019**, *1*, 83.
- [49] S. Ghosh, V. Gueskine, M. Berggren, I. V. Zozoulenko, J. Phys. Chem. C 2019, 123, 15467.
- [50] J. Rivnay, S. C. B. Mannsfeld, C. E. Miller, A. Salleo, M. F. Toney, *Chem. Rev.* 2012, 112, 5488.
- [51] X. Zhang, L. J. Richter, D. M. Delongchamp, R. J. Kline, M. R. Hammond, I. McCulloch, M. Heeney, R. S. Ashraf, J. N. Smith, T. D. Anthopoulos, B. Schroeder, Y. H. Geerts, D. A. Fischer, M. F. Toney, *J. Am. Chem. Soc.* 2011, *133*, 15073.
- [52] Y. Xi, C. M. Wolf, L. D. Pozzo, Soft Matter 2019, 15, 1799.
- [53] D. Khodagholy, J. Rivnay, M. Sessolo, M. Gurfinkel, P. Leleux, L. H. Jimison, E. Stavrinidou, T. Herve, S. Sanaur, R. M. Owens, G. G. Malliaras, *Nat. Commun.* **2013**, *4*, 2133.
- [54] X. Wu, A. Surendran, M. Moser, S. Chen, B. T. Muhammad, I. P. Maria, I. Mcculloch,W. L. Leong, ACS Appl. Mater. Interfaces 2020, 12, 20757.
- [55] R. Steyrleuthner, Y. Zhang, L. Zhang, F. Kraffert, B. P. Cherniawski, R. Bittl, A. L. Briseno, J. L. Bredas, J. Behrends, *Phys. Chem. Chem. Phys.* **2017**, *19*, 3627.
- [56] H. Sun, M. Vagin, S. Wang, X. Crispin, R. Forchheimer, M. Berggren, S. Fabiano, Adv. Mater. 2018, 30, 1704916.
- [57] E. Zeglio, M. M. Schmidt, M. Thelakkat, R. Gabrielsson, N. Solin, O. Inganäs, *Chem. Mater.* **2017**, *29*, 4293.
- [58] D. Beatrup, J. Wade, L. Biniek, H. Bronstein, M. Hurhangee, J. S. Kim, I. McCulloch,J. R. Durrant, *Chem. Commun.* 2014, 50, 14425.